Entropic lattice Boltzmann representations required to recover Navier-Stokes flows

Brian Keating and George Vahala
Department of Physics, William & Mary, Williamsburg, Virginia 23187, USA

Jeffrey Yepez
Air Force Research Laboratories, Hanscom Field, Massachusetts 02139, USA

Min Soe
Department of Mathematics & Science, Rogers State University, Claremore, Oklahoma 74017, USA

Linda Vahala
Department of Electrical & Computer Engineering, Old Dominion University, Norfolk, Virginia 23529, USA

(Received 3 August 2006; revised manuscript received 5 December 2006; published 29 March 2007)

There are two disparate formulations of the entropic lattice Boltzmann scheme: one of these theories revolves around the analog of the discrete Boltzmann H function of standard extensive statistical mechanics, while the other revolves around the nonextensive Tsallis entropy. It is shown here that it is the nonenforcement of the pressure tensor moment constraints that lead to extremizations of entropy resulting in Tsallis-like forms. However, with the imposition of the pressure tensor moment constraint, as is fundamentally necessary for the recovery of the Navier-Stokes equations, it is proved that the entropy function must be of the discrete Boltzmann form. Three-dimensional simulations are performed which illustrate some of the differences between standard lattice Boltzmann and entropic lattice Boltzmann schemes, as well as the role played by the number of phase-space velocities used in the discretization.

DOI: 10.1103/PhysRevE.75.036712 PACS number(s): 47.11.Qr, 47.27.E−, 47.10.ad

I. INTRODUCTION

The lattice Boltzmann (LB) approach to low-Mach-number Navier-Stokes flows (because of its simplicity, its nearly perfect parallelization on supercomputers platforms and the ease with which difficult boundary conditions can be handled) deserves considerable attention [1]. The LB approach, in its simplest form, is a discretized linearized Boltzmann equation with BGK collisional relaxation. Moreover, to minimize the number of degrees of freedom in kinetic velocity space one chooses a kinetic lattice with a sufficient number of velocities so that in the long-wavelength long-time (Chapman-Enskog) limit the discrete symmetry LB approach recovers the nonlinear continuum macroscopic equations. In this paper we will be examining LB models that recover the quasi-incompressible Navier-Stokes equations

$$\frac{\partial \rho}{\partial t} + \nabla \cdot (\rho \mathbf{u}) = 0,$$

$$\rho\left(\frac{\partial \mathbf{u}}{\partial t} + \mathbf{u} \cdot \nabla \mathbf{u}\right) = -\nabla p + \nu \nabla^2 \mathbf{u}, \tag{1}$$

where ρ is the density, $\mathbf{u}$ the mean fluid velocity, and ν is the viscosity. In the quasi-incompressible limit $\rho \approx$ const in the continuity equation, and under the isothermal constraint the pressure $p = \rho c_s^2$, where c_s is the (constant) sound speed. We will also make some comments on the Burgers equation: Eq. (1) with $\nabla p \equiv 0$. LB projects the problem onto kinetic space $(\mathbf{x}, \boldsymbol{\xi}, t)$ and determines the evolution of the distribution function $f(\mathbf{x}, \boldsymbol{\xi}, t)$ from the linearized BGK-collision term

$$\frac{\partial f}{\partial t} + \boldsymbol{\xi} \cdot \nabla f = -\frac{1}{\tau}(f - f^{eq}), \tag{2}$$

where τ is the relaxation rate at which f relaxes to the "equilibrium" distribution function f^{eq}. Both τ and f^{eq} are free parameters and functions. Under appropriate lattice discretization of the phase-space velocity $\boldsymbol{\xi}$ (see below for more detail), the simplest explicit algorithm to solve Eq. (2) is

$$f_\alpha(\mathbf{x} + \mathbf{e}_\alpha, t+1) - f_\alpha(\mathbf{x}, t) = -\frac{1}{\tau}[f_\alpha(\mathbf{x}, t) - f_\alpha^{eq}(\mathbf{x}, t)]. \tag{3}$$

Here $\alpha = 1, \ldots, Q$, where Q is the number of lattice velocity vectors $\mathbf{e}_\alpha$ or "bits" for the chosen underlying lattice. Standard LB units have been chosen in which $\Delta x = 1 = \Delta t$, and we are here considering the simplest case of congruent spatial and lattice grids. On performing Chapman-Enskog asymptotics on the LB equation (3), one recovers the Navier-Stokes equations (1), provided f^{eq} satisfies certain constraints. The transport coefficient

$$\nu = \frac{1}{6}(2\tau - 1), \tag{4}$$

while the standard moments connect the variables in the mesoscopic (LB) and macroscopic (Navier-Stokes) descriptions:

$$\rho = \sum_{\alpha=1}^{Q} f_\alpha^{eq} = \sum_{\alpha=1}^{Q} f_\alpha, \quad \rho \mathbf{u} = \sum_{\alpha=1}^{Q} f_\alpha^{eq} \mathbf{e}_\alpha = \sum_{\alpha=1}^{Q} f_\alpha \mathbf{e}_\alpha. \tag{5}$$

There are some striking features when comparing these two representations.

(i) The nonlinear convective derivatives of Navier-Stokes equation are now replaced by simple linear advection in the kinetic representation.

(ii) The nonlinear differential operators of the Navier-Stokes equation are reproduced by simple local algebraic functions in f^{eq}.

The LB algorithm, as can be seen from Eq. (3), consists of primarily two steps: (a) Free-streaming the distribution f_α from $\mathbf{x}$ to $\mathbf{x}+\mathbf{e}_\alpha$, for each $\alpha=1,\ldots,Q$, followed by (b) local collisional relaxation. As a result, the LB algorithm is ideally vectorized and parallelized on multiprocessor architectures [2].

The Achilles' heel of the LB approach is numerical instabilities arising particularly in high-Reynolds-number flows. These instabilities arise in the standard LB approach since there are no constraints imposed on the evolution of the distribution functions to ensure their non-negative behavior at every grid point for all times. Recently, there have been two seemingly disparate approaches advocated by what we shall call the Zurich school [3–8] and the Boston school [9–12]. These groups both introduced a discrete *H*-theorem constraint which enforces positive-definiteness on the distribution functions. These methods are termed entropic lattice Boltzmann (ELB) methods and lead to unconditionally stable explicit algorithms at arbitrary small viscosity. In particular, the Zurich school [3–8] works with a discretized weighted form of the continuum Boltzmann *H* function, while the Boston school [9–12] bases their work on a Tsallis [13] entropy function. There are fundamental differences between these two entropy functions: while the Tsallis entropy will tend to the discrete Boltzmann entropy in a special limit, away from this limit the Tsallis entropy is nonextensive and is indicative of underlying special microscopic dynamics due to either nonergodicity, fractal spatiotemporal structures, or long-range interactions. The discrete Boltzmann entropy, on the other hand, is extensive. Boghosian [14] has initiated an attempt to reconcile the extensive Zurich and nonextensive Boston approaches. Here we complete this reconciliation and show explicitly that the constraint on the pressure tensor, necessary to recover the Navier-Stokes equations, will force the entropy to take the extensive Boltzmann form. Without this pressure constraint being enforced, the nonextensive Tsallis-like entropy can be found.

In Sec. II, we review the standard polynomial equilibrium relaxation distribution functions used in the LB approach for the D3Q15, D3Q19, and D3Q27 models [where D3Q15 represents the three-dimensional (3D), 15-velocity model, etc.], and in Sec. III we review carefully the approaches of the Zurich [3–8] and Boston [9–12] schools, as well as the unifying approach of Boghosian [14]. In Sec. IV, starting with the unifying approach of Boghosian we show that the pressure tensor constraint plays a pivotal role in the form of the discrete *H* function so as to recover the Navier-Stokes equation, while in Sec. V we present some preliminary simulations comparing and contrasting the ELB versus LB algorithms as well as the role of the number of velocity bits in the algorithm. In Sec. VI we present some concluding remarks.

TABLE I. A summary of the D3Q15, D3Q19, and D3Q27 lattice models. The number of velocity "bits" for given speeds are given inside the $(\cdots)$ of the first column. The second column gives the base lattice velocity on which the permutations are performed, while the weights w_α are given in columns 3–5.

Speed (No. velocities)	Velocities (permutation on)	3DQ15	3DQ19	3DQ27
Rest (1)	(0, 0, 0)	$w_0=\frac{2}{9}$	$w_0=\frac{1}{9}$	$w_0=\frac{8}{27}$
1 (6)	$(\pm1,0,0)$	$w_1=\frac{1}{9}$	$w_1=\frac{1}{18}$	$w_2=\frac{2}{27}$
$\sqrt{2}$ (12)	$(\pm1,\pm1,0)$	$w_2=0$	$w_2=\frac{1}{36}$	$w_2=\frac{1}{54}$
$\sqrt{3}$ (8)	$(\pm1,\pm1,\pm1)$	$w_3=\frac{1}{72}$	$w_3=0$	$w_3=\frac{1}{216}$

II. STANDARD LB RELAXATION DISTRIBUTION FUNCTIONS

There are two sets of free functions in the standard LB equation (3): the relaxation distribution functions f_α^{eq} and the relaxation rate τ which determines the viscosity, Eq. (4). In the LB approach, τ is a constant while the Q distributions f_α^{eq}, $\alpha=1,\ldots,Q$ (due to standard assumptions in the Chapman-Enskog theory), are functions of the conserved collisional moments $\rho,\rho\mathbf{u}$. The Navier-Stokes equations are recovered in the long-wavelength long-time limit for the 3D lattices D3Q15, D3Q19, and D3Q27 (detailed in Table I) provided the relaxation distribution functions are chosen in the form

$$f_\alpha^{eq}(\mathbf{x},t)=\rho w_\alpha\Bigg[1+3\mathbf{e}_\alpha\cdot\mathbf{u}+\frac{9}{2}(\mathbf{e}_\alpha\cdot\mathbf{u})^2-\frac{3}{2}\mathbf{u}\cdot\mathbf{u}+\frac{9}{2}(\mathbf{e}_\alpha\cdot\mathbf{u})\times\{(\mathbf{e}_\alpha\cdot\mathbf{u})^2-\mathbf{u}\cdot\mathbf{u}\}\Bigg]+O(u^4), \tag{6}$$

with $\alpha=1,\ldots,Q$. Only the weights w_α change with the choice of the number of velocities in the model, as seen in Table I, while the form of f_α^{eq} remains invariant. For our simulations the $O(u^3)$ terms in Eq. (6) are incorporated. It seems that they are not only important in high-Knudsen-number flows of relevance to microchannel flows [15] but they will be related to the ELB form of the distribution function, as we shall soon see.

The leading moments of the Maxwellian distribution for incompressible flow are (in discrete kinetic velocity representation)

$$\sum_{\alpha=1}^{Q}f_\alpha^{eq}=\rho,\quad \sum_{\alpha=1}^{Q}f_\alpha^{eq}e_{\alpha,i}=\rho u_i,$$

$$\sum_{\alpha=1}^{Q}f_\alpha^{eq}e_{\alpha,i}e_{\alpha,j}=p\,\delta_{ij}+\rho u_i u_j,\quad \text{with } p=\rho c_s^2=\frac{1}{3}\rho,$$

$$\sum_{\alpha=1}^{Q}f_\alpha^{eq}e_{\alpha,i}e_{\alpha,j}e_{\alpha,k}=\frac{1}{3}\rho(u_i\delta_{jk}+u_j\delta_{ki}+u_k\delta_{ij})+\rho u_i u_j u_k. \tag{7}$$

Here the Greek α is the index for the different phase-space velocities, while the Roman indices (i,j,k) give the Cartesian component of that vector field. Since the LB systems for Navier-Stokes flows are closed at the second moment, one can view the third moment as somewhat superfluous. One readily verifies that the relaxation distribution functions, Eq. (6), for all three models D3Q15, D3Q19, and D3Q27 with the weights given in Table I satisfy the moments in Eq. (7) except for the diagonal components of the third-rank tensor where now

$$\sum f_\alpha^{eq} e_{\alpha,i} e_{\alpha,i} e_{\alpha,i} = \rho u_i; \tag{8}$$

i.e., there are errors of order $O(u^3)$ in these diagonal moments, indicating a loss of Galilean invariance at $O(u^3)$. For low Mach numbers ($\mathrm{Ma} < 0.1$), these corrections are very small.

The standard LB scheme loses numerical stability as the Reynolds number $\mathrm{Re} = U_0 L_0 / \nu$ increases (i.e., as $\tau \to 0.5_+$) since at some grid point $\mathbf{x}'$ and time $t' f_\alpha(\mathbf{x}', t') < 0$.

III. ENTROPIC LB REPRESENTATIONS OF THE ZURICH AND BOSTON SCHOOLS

In an ELB representation one requires in the dynamical evolution of the distribution functions that the Lyapunov H function

$$H = \sum_{\alpha=1}^{Q} h_\alpha(f_\alpha) \tag{9}$$

never decrease. h_α are convex functions, with $h_\alpha'(z) \geqslant 0$ for all $z > 0$. The relaxation distribution function f_α^{eq} extremize the H function subject to the local collisional invariants of mass and momentum, Eq. (5). Introducing the corresponding Lagrange multipliers $(\mu(\mathbf{x},t), \boldsymbol{\beta}(\mathbf{x},t))$, the extremization of

$$\delta \sum_{\alpha=1}^{Q} [h_\alpha(f_\alpha) - \mu f_\alpha - \beta \cdot f_\alpha \mathbf{e}_\alpha] = 0 \tag{10}$$

yields

$$h_\alpha'(f_\alpha^{eq}) = \mu + \beta \cdot \mathbf{e}_\alpha, \quad \alpha = 1, \ldots, Q. \tag{11}$$

A. Zurich school

The Zurich school [3–8] has formulated their ELB using two different but equivalent approaches. In their first approach the discrete H function is derived upon applying Gauss-Hermite quadratures on the standard continuum Boltzmann H function, yielding

$$H_B[f_\alpha] = \sum_{\alpha=1}^{Q} f_\alpha \ln\left(\frac{f_\alpha}{w_\alpha}\right), \tag{12}$$

where w_α are the weights given in Table I for the D3Q27 model. On extremizing Eq. (12) subject to the local collisonal moment constraints of mass and momentum, one obtains exponential forms for the f_α^{eq} with the Lagrange multipliers $(\mu, \boldsymbol{\beta})$. These f_α^{eq} are then substituted into the moment expressions for ρ and $\rho \mathbf{u}$ in order to determine the Lagrange multipliers. The Zurich school [3–8] has then obtained explicit (exact) solutions for the Lagrange multipliers with f_α^{eq} given by

$$f_\alpha^{eq} = \rho w_\alpha \prod_{i=1}^{3} (2 - \sqrt{1 + 3u_i^2}) \left(\frac{2u_i + \sqrt{1 + 3u_i^2}}{1 - u_i}\right)^{e_{\alpha,i}}, \quad \alpha = 1, \ldots, 27. \tag{13}$$

The square root arises from the positive root of a quadratic equation. It can be readily verified that this relaxation distribution function f_α^{eq} for D3Q27 satisfies the moment equations (7)—except for the diagonal terms of the third-rank tensor which satisfy Eq. (8)—just as the Taylor-expanded standard LB f_α^{eq}, Eq. (6).

Interestingly, we find that the D3Q15 and D3Q19 forms of Eq. (14), with the corresponding weights in Table I, also satisfy the moments, Eq. (7), except for the diagonal terms of the third-rank tensor that satisfy Eq. (8). Even though one cannot determine the Lagrange multipliers explicitly for the D3Q15 and D3Q19 systems, these moments of Eq. (13) differ from the moments of the Taylor-expanded f_α^{eq} only to terms of $O(u^4)$. Most likely the exact entropic D3Q27 model exists since it is the tensor product of the exactly soluble D1Q3 case, where as the D3Q15 and D3Q19 cases are not.

In their second approach the Zurich school [3–8] first applies symmetry arguments so that the h_α in Eq. (9) are only dependent on α when moving at a different speed. Thus, for 3DQ27 there are four different h_α functions. The extremizing of the H function, subject to the local collisional conservation of mass and momentum, yields Eq. (11). On defining the inverse function (which must exist due to the convexity property of h_α)

$$h_\alpha'^{-1} = \phi_\alpha, \tag{14}$$

a formal inverse of Eq. (11) is

$$f_\alpha^{eq} = \phi_\alpha(\mu + \mathbf{e}_\alpha \cdot \beta). \tag{15}$$

The functions ϕ_α are determined so that the pressure tensor moment is satisfied up to second order in Mach number: i.e., if one introduces the second moment error tensor ε_{ij},

$$\varepsilon_{ij} = \sum_{\alpha=1}^{Q} \phi_\alpha(\mu + \mathbf{e}_\alpha \cdot \beta) e_{\alpha,i} e_{\alpha,j} - \rho c_s^2 \delta_{ij} - \rho u_i u_j, \tag{16}$$

then one requires that $\varepsilon_{ij} = O(u^3)$. This will determine the h_α function, the value of the sound speed (for self-consistency) $c_s = 1/\sqrt{3}$, and the weights w_α. One obtains the discrete H function of Eq. (12), with the weights given in Table I.

B. Boston school

The Boston school [9–12] also extremizes Eq. (9) subject to the collisional invariants of mass and momentum, and this yields the inverse function $h_\alpha'^{-1}$ with formal inverse Eq. (15):

$$f_\alpha^{eq} = \phi_\alpha(\mu + \mathbf{e}_\alpha \cdot \beta).$$

Boghosian [14] now proceeds somewhat differently from the second approach of the Zurich school [3–8]. He demands lattice isotropy constraints on the $\phi_\alpha(\mu)$ for the chosen lattice geometry vectors $\mathbf{e}_\alpha$:

$$\sum_{\alpha=1}^{Q} \phi_\alpha(\mu) = \Phi_0(\mu),$$

$$\sum_{\alpha=1}^{Q} \phi_\alpha(\mu) e_{\alpha,i} = 0,$$

$$\sum_{\alpha=1}^{Q} \phi_\alpha(\mu) e_{\alpha,i} e_{\alpha,j} = \Phi_2(\mu)\delta_{ij},$$

$$\sum_{\alpha=1}^{Q} \phi_\alpha(\mu) e_{\alpha,i} e_{\alpha,j} e_{\alpha,k} = 0,$$

$$\sum_{\alpha=1}^{Q} \phi_\alpha(\mu) e_{\alpha,i} e_{\alpha,j} e_{\alpha,k} e_{\alpha,\ell} = \Phi_4(\mu)[\delta_{ij}\delta_{k\ell} + \delta_{ik}\delta_{\ell j} + \delta_{i\ell}\delta_{jk}], \tag{17}$$

for some functions $\Phi_0(\mu)$, $\Phi_2(\mu)$, and $\Phi_4(\mu)$. Note that these isotropy constraints are enforced about $\mathbf{u}=0$—again, the low-Mach-number expansion, common to all LB and ELB schemes. The Boston school [9–12] performs a Taylor expansion of the relaxation distribution functions, Eq. (15), in powers of small $\boldsymbol{\beta}$ [it can be shown that $\boldsymbol{\beta}=O(u)$]. The forms of the Lagrange multipliers are determined on substituting these expanded f_α^{eq} into the collisional moment constraints, Eq. (5). After Chapman-Enskog expansions, one finally determines the momentum continuum equation [9–12]

$$\frac{\partial \mathbf{u}}{\partial t} + g\mathbf{u} \cdot \boldsymbol{\nabla}\mathbf{u} = -\boldsymbol{\nabla}P + \nu\nabla^2\mathbf{u}, \tag{18}$$

where the Galilean prefactor g in front of the nonlinear convective derivative is

$$g = \frac{\Phi_0\Phi_4''}{[\Phi_2']^2}, \tag{19}$$

while the pressure P is given by

$$P = \Phi_2 + \frac{\rho\mathbf{u}^2}{2}\left[\frac{\Phi_0\Phi_4''}{(\Phi_2')^2} - \frac{\Phi_0\Phi_2''}{\Phi_0'\Phi_2'}\right]. \tag{20}$$

To ensure Galilean invariance, the Boston school [9–12] enforces the constraint

$$g = \frac{\Phi_0\Phi_4''}{[\Phi_2']^2} = 1. \tag{21}$$

Then, on taking the trace of the isotropy constraints, Eq. (17), and using Eq. (16), Boghosian [14] shows that Galilean invariance, Eq. (21), is satisfied provided

$$\left[\sum_{\alpha=1}^{Q} \phi_\alpha(\mu)\right]\left[\sum_{\alpha=1}^{Q} \phi_\alpha''(\mu)|\mathbf{e}_\alpha|^4\right] = \frac{5}{3}\left[\sum_{\alpha=1}^{Q} \phi_\alpha'(\mu)|\mathbf{e}_\alpha|^2\right]^2. \tag{22}$$

This constraint equation for $\phi_\alpha = h_\alpha'^{-1}$ is solved by a power-law solution

$$\phi_\alpha(\mu) = \bar{w}_\alpha(\mu - b)^\gamma, \tag{23}$$

where $\bar{w}_\alpha$ are some weights to be determined, b is an arbitrary constant, and γ is an exponent that will be related to the Tsallis q parameter [5] of nonextensive entropy. On substituting Eq. (23) into Eq. (22) one obtains the relationship

$$\frac{5}{3}\frac{\gamma}{\gamma - 1} = \frac{\left[\sum_{\alpha=1}^{Q} \bar{w}_\alpha\right]\left[\sum_{\alpha=1}^{Q} \bar{w}_\alpha|\mathbf{e}_\alpha|^4\right]}{\left[\sum_{\alpha=1}^{Q} \bar{w}_\alpha|\mathbf{e}_\alpha|^2\right]^2}. \tag{24}$$

This yields the discrete H function, Eq. (9), on disregarding the irrelevant constant of integration [5]:

$$H = \sum_{\alpha=1}^{Q} h_\alpha(f_\alpha) = \sum_{\alpha=1}^{Q} z\left[b + \frac{\gamma}{1+\gamma}\left(\frac{f_\alpha}{\bar{w}_\alpha}\right)^{1/\gamma}\right]. \tag{25}$$

By appropriate choice of b, this can be rewritten in the form

$$H = (2-q)(1-q)\sum_{\alpha=1}^{Q} f_\alpha\left[\frac{\left(\frac{f_\alpha}{\bar{w}_\alpha}\right)^{1-q} - 1}{1-q}\right]$$

$$\equiv (2-q)(1-q)\sum_{\alpha=1}^{Q} f_\alpha \ln_q\left(\frac{f_\alpha}{\bar{w}_\alpha}\right), \tag{26}$$

where the generalized logarithmic function

$$\ln_q z \equiv \frac{z^{1-q} - 1}{1-q} \to \ln z, \quad \text{as } q \to 1, \tag{27}$$

and the Tsallis q parameter

$$q = 1 - \frac{1}{\gamma}. \tag{28}$$

In the nonextensive limit $q \to 1$, the summation term in Eq. (27) tends to the Zurich school's H function, Eq. (12), with the weights $\bar{w}_\alpha \to w_\alpha$, the weights given in Table I. In this nonextensive limit $\gamma \to \infty$.

Boghosian [14] does comment that it is somewhat surprising to recover a Tsallis entropic form as the generic form for the ELB equation since the Tsallis entropy typically arises from nonergodicity or fractal spatiotemporal systems or systems with long-range interactions [16]. However, the LB formalism does not necessarily have any such special dynamics.

It should be noted that the $(1-q)$ factor in Eq. (27) makes a nontrivial, nonextensive $q \to 1$ limit somewhat problematic. The occurrence of the Tsallis entropy may possibly be correlated to the existence of the unphysical $\mathbf{u}^2$ term in the pressure term P, Eq. (20), since the power-law solution, Eq. (23), with Eq. (21) results in

$$\frac{\Phi_0\Phi_4''}{(\Phi_2')^2} - \frac{\Phi_0\Phi_2''}{\Phi_0'\Phi_2'} = 1 - \frac{\Phi_0\Phi_2''}{\Phi_0'\Phi_2'} \neq 0. \tag{29}$$

IV. ENTROPIC LB RELAXATION DISTRIBUTION FUNCTION

We now extend the Boghosian [14] Galielan-invariant unifying theory by requiring the pressure P to be physical: i.e., we require the coefficient of the $\mathbf{u}^2$ term in Eq. (20) to vanish:

$$\frac{\Phi_0\Phi_2''}{\Phi_0'\Phi_2'} = 1. \tag{30}$$

We assume a form similar to Boghosian:

$$\phi_\alpha(\mu) = w_\alpha F(\mu), \tag{31}$$

where the weights w_α and function F are to be determined. Explicitly writing out the even isotropic lattice moment constraints of Eq. (17), we find

$$\sum_{\alpha=1}^{Q} \phi_\alpha(\mu) = (w_0 + 6w_1 + 12w_2 + 8w_3)F(\mu) \equiv \Phi_0(\mu),$$

$$\sum_{\alpha=1}^{Q} \phi_\alpha(\mu) e_{\alpha,i} e_{\alpha,j} = (2w_1 + 8w_2 + 8w_3)\delta_{ij} F(\mu) \equiv \Phi_2(\mu)\delta_{ij},$$

$$\sum_{\alpha=1}^{Q} \phi_\alpha(\mu) e_{\alpha,i} e_{\alpha,j} e_{\alpha,k} e_{\alpha,\ell} = [\Lambda_{ijk\ell}(4w_2 + 8w_3) + \delta_{ijk\ell}(2w_1 - 4w_2 - 16w_3)]F(\mu) \equiv \Phi_4(\mu)\Lambda_{ijk\ell} \tag{32}$$

where the isotropic fourth-rank tensor $\Lambda_{ijk\ell} = \delta_{ij}\delta_{k\ell} + \delta_{ik}\delta_{j\ell} + \delta_{i\ell}\delta_{jk}$ and the anisotropic fourth-rank tensor $\delta_{ijk\ell} = 1$ iff $i = j = k = \ell$ (otherwise it is zero). Equation (32) is valid for any of the D3Q15, D3Q19, and D3Q27 models: for D3Q15 there are no speed $\sqrt{2}$ velocities so that $w_2 = 0$, while for D3Q19 there are no speed $\sqrt{3}$ velocities so that $w_3 = 0$.

For isotropy the coefficient of $\delta_{ijk\ell}$ must be zero:

$$w_1 - 2w_2 - 8w_3 = 0. \tag{33}$$

We now impose both the Galilean constraint, Eq. (21), and that the pressure be independent of the mean velocity, Eq. (20):

$$g = \frac{\Phi_0\Phi_4''}{[\Phi_2']^2} = 1 = \frac{\Phi_0\Phi_2''}{\Phi_0'\Phi_2'}. \tag{34}$$

From Eq. (32) the pressure constraint immediately yields an equation for $F(\mu)$,

$$F''(\mu)F(\mu) = [F'(\mu)]^2, \tag{35}$$

while the Galilean constraint places a constraint on the weights:

$$(w_0 + 6w_1 + 12w_2 + 8w_3)(4w_2 + 8w_3) = (2w_1 + 8w_2 + 8w_3)^2. \tag{36}$$

One typically introduces a normalization constraint on the w_α:

$$w_0 + 6w_1 + 12w_2 + 8w_3 = 1, \tag{37}$$

and, finally, on physical grounds we require $w_\alpha \geqslant 0$. [The odd lattice moment constraints of Eq. (17) are trivially satisfied for weights that are only speed dependent.]

Equations (33), (36), and (37) are three constraint equations for (at most) four unknown weights w_α [17]. It is easily verified that the D3Q27 weights in Table I satisfy these constraint equations, while for the D3Q15 and D3Q19 models the unique solutions of Eqs. (33), (36), and (37) are the weights given in Table I.

Finally, we determine the relaxation distribution function in a low-Mach-number expansion, following Boghosian [14] and the Boston school [9–12]. A solution to Eq. (35)—an equation that occurs repeatedly in the Zurich school ELB—is a simple exponential

$$F(\mu) = e^\mu, \tag{38}$$

so that Eq. (32) yields

$$\Phi_0(\mu) = e^\mu, \quad \Phi_2(\mu) = \frac{1}{3}e^\mu, \quad \Phi_4(\mu) = \frac{1}{9}e^\mu. \tag{39}$$

The details of how to determine the Lagrange multiplier μ and $\boldsymbol{\beta}$ by a low-Mach-number Taylor expansion of the relaxation distribution function moments are given in detail in Refs. [9–12,14], and will not be repeated here. To leading order,

$$\Phi_0 = e^\mu = \rho + O(\beta^2), \quad \text{with } \beta = O(\mathbf{u}), \tag{40}$$

so that

$$\Phi_0^{-1}(\rho) = \ln\rho + \cdots. \tag{41}$$

To second order in Mach number, the Taylor-expanded relaxation distribution function [9–12,14]

$$f_\alpha^{eq} = \phi_\alpha + \frac{\phi_\alpha'}{\Phi_2'}\rho e_{\alpha,i}u_i + \frac{\rho u_i u_j}{2(\Phi_2')^2}\left[\phi_\alpha'' e_{\alpha,i}e_{\alpha,j} - \phi_\alpha'\frac{\Phi_2''}{\Phi_0'}\delta_{ij}\right] + O(u^3), \tag{42}$$

where all the ϕ's and Φ's are evaluated at $\Phi_0^{-1}(\rho) = \ln\rho$. Since $\phi_\alpha(\ln\rho) = w_\alpha \exp(\ln\rho) = w_\alpha\rho$, we have $\phi_\alpha'(\ln\rho) = w_\alpha\rho = \phi_\alpha''(\ln\rho)$, $\Phi_0'(\ln\rho) = \rho$, $\Phi_2'(\ln\rho) = \rho/3 = \Phi_2''(\ln\rho)$ so that the relaxation distribution function, Eq. (42), becomes

$$f_\alpha^{eq} = \rho w_\alpha\left[1 + 3\mathbf{u}\cdot\mathbf{e}_\alpha + \frac{9}{2}(\mathbf{u}\cdot\mathbf{e}_\alpha)^2 - \frac{3}{2}\mathbf{u}^2 + O(u^3)\right], \tag{43}$$

which is just the standard polynomial form of the relaxation distribution function, Eq. (6). Equation (43) applies to all

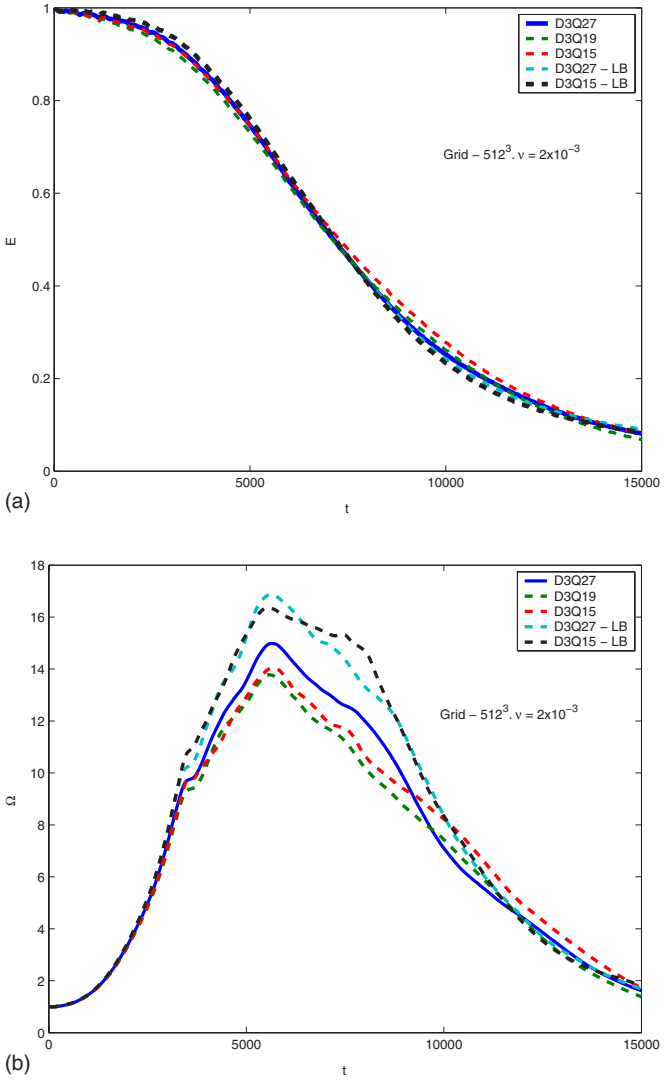

FIG. 1. (Color online) The decay of the (a) normalized kinetic energy and the (b) normalized enstrophy for the viscosity run $\nu = 2 \times 10^{-3}$ using the LB and ELB algorithms for D3Q15, D3Q19, and D3Q27. Time is in units of LB iterations, and the spatial grid is 512^3. These simulations are fully resolved at Re=2037, with integral to dissipation length scales $L/\ell_D \approx \mathrm{Re}^{3/4} \approx 300$. The kinetic energy decay is insensitive to whether the simulation uses the LB or ELB algorithm as well as the number of velocity bits in the model. However, the enstrophy decay shows dependence on both the algorithm and bit model used in the simulation. Since the ELB viscosities are somewhat higher than the corresponding LB bare viscosities, the LB enstrophy maxima (which are controlled by the viscosity) are greater than for ELB. The rapid rise in the enstrophy for early times is due to vortex stretching, which is independent of the viscosity.

three models D3Q15, D3Q19, and D3Q27, with weights given in Table I. The H function is

$$H[\mathbf{f}] = \sum_{\alpha=1}^{Q} f_\alpha \ln\left(\frac{f_\alpha}{w_\alpha}\right), \tag{44}$$

while the pressure P, from Eqs. (20), (24), and (39),

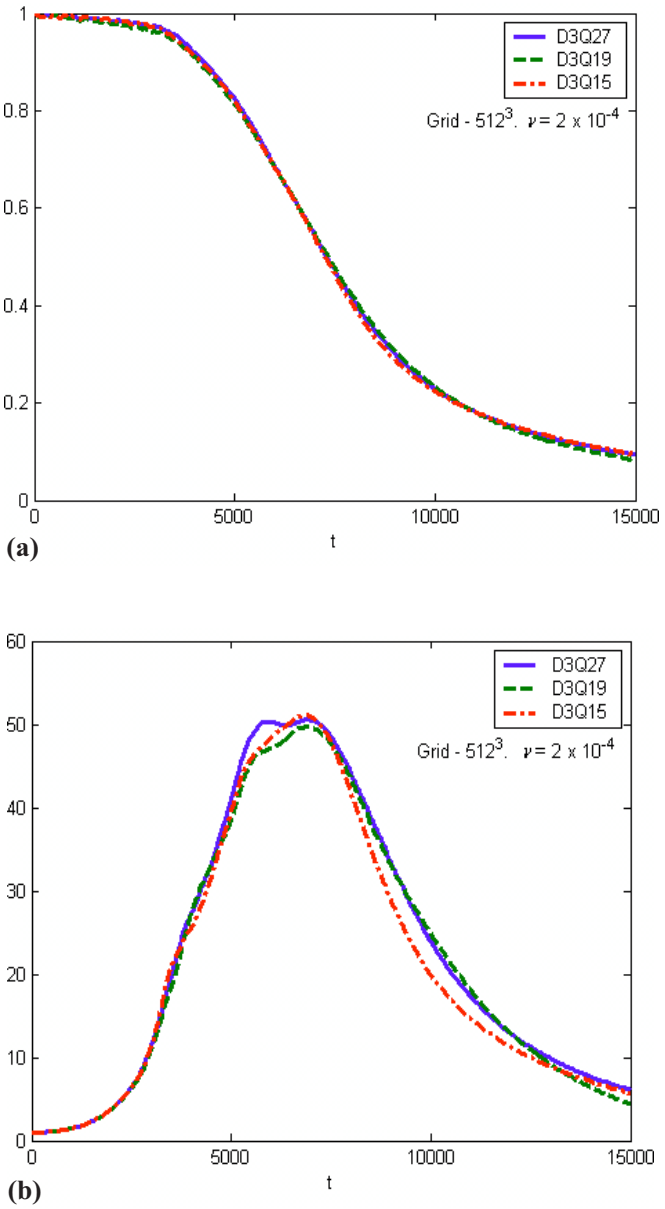

FIG. 2. (Color online) The decay of the (a) normalized kinetic energy and the (b) normalized enstrophy for the lower viscosity run $\nu = 2 \times 10^{-4}$. At this viscosity the standard LB algorithm rapidly becomes numerically unstable. The ELB algorithm is unconditionally stable for all viscosities. These runs at Re=20 370 are somewhat under-resolved ($L/\ell_D \approx 1700$). Both the energy and enstrophy evolution now show little variation with bit model. The enstrophy maxima are now enhanced by over a factor of 3 from those in Fig. 1 due to the reduced viscosity.

$$P = \Phi_2(\ln \rho) = \frac{1}{3}\rho, \tag{45}$$

with the sound speed $c_s^2 = 1/3$ and the kinematic viscosity—from Chapman Enskog expansions [9–12] of Eq. (3):

$$\nu = \frac{\Phi_4'}{2\Phi_2'}(2\tau - 1) = \frac{1}{6}(2\tau - 1), \tag{46}$$

in agreement with Eq. (4).

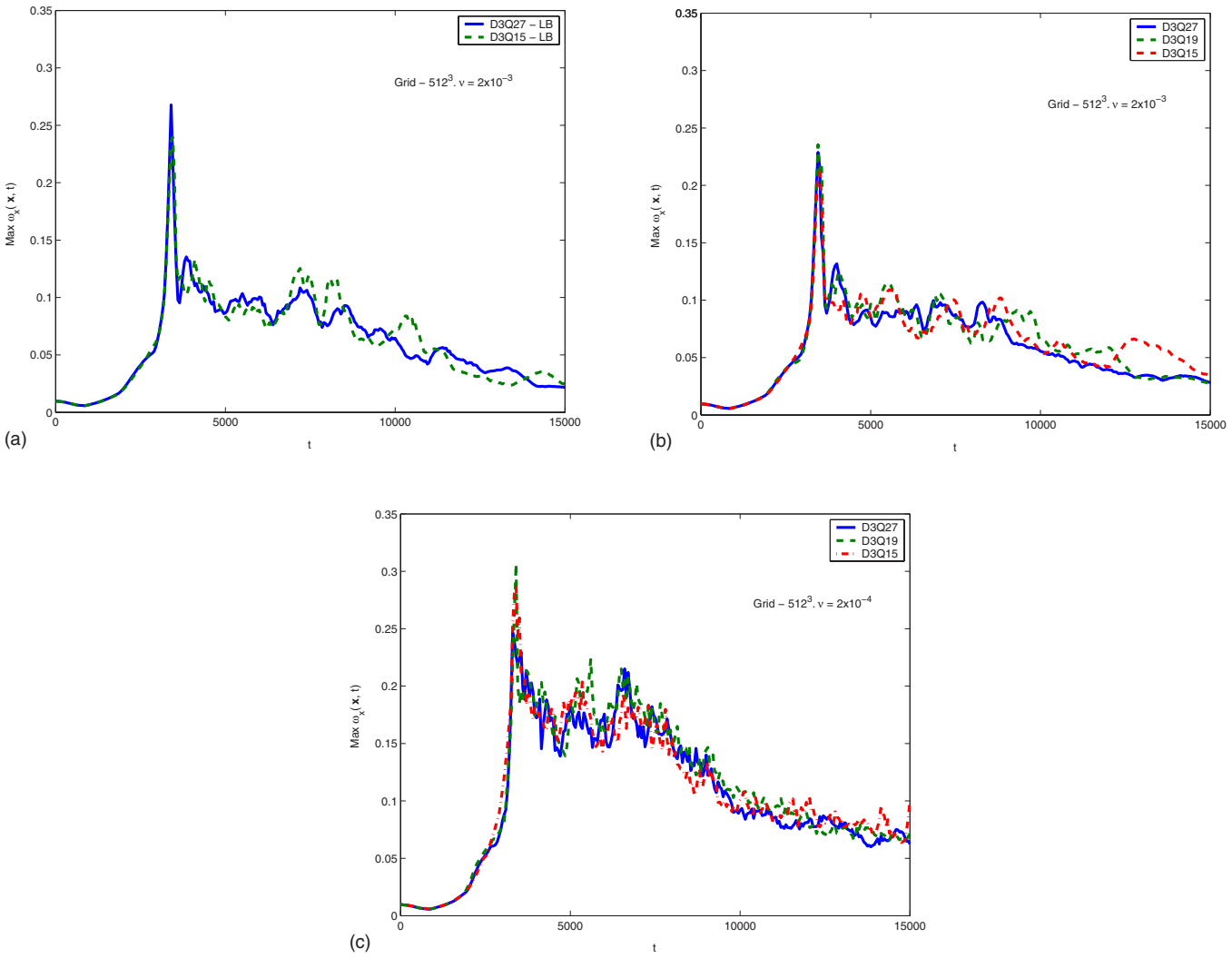

FIG. 3. (Color online) The time evolution of $\hat{\omega}(t)=\max_{\mathbf{x}}\omega_x(\mathbf{x},t)$ where $\omega_x=\hat{\mathbf{x}}\cdot(\boldsymbol{\nabla}\times\mathbf{u})$ is the x component of vorticity for the various velocity bit models: D3Q27, D3Q19, and D3Q15 models. The spatial grid is 512^3. (a) LB at $\nu=2\times10^{-3}$, (b) ELB at $\nu=2\times10^{-3}$, and (c) ELB at $\nu=2\times10^{-4}$. For early times there is strong vortex stretching that is independent of viscosity. There are some bit-model variations in both the LB and ELB runs at $\nu=2\times10^{-3}$, but these are not present for the ELB simulation at the lower viscosity $\nu=2\times10^{-4}$.

V. PRELIMINARY SIMULATIONS OF THE ELB FOR NAVIER-STOKES TURBULENCE: D3Q15, D3Q19, AND D3Q27 MODELS

One form of the ELB approach [3–8], which enforces the positive-definiteness of the f_α at each grid point for all time, generalizes the simple one-parameter BGK collision term in Eq. (3) to a two-parameter collision term

$$f_\alpha(\mathbf{x}+\mathbf{e}_\alpha,t+1)-f_\alpha(\mathbf{x},t)=-\frac{\gamma(\mathbf{x},t)}{2\tau}[f_\alpha(\mathbf{x},t)-f_\alpha^{eq}(\mathbf{x},t)]. \quad (47)$$

The function $\gamma(\mathbf{x},t)$ is the nontrivial root of

$$H[\mathbf{f}]=H[\mathbf{f}-\gamma(\mathbf{f}-\mathbf{f}^{eq})], \quad (48)$$

so that entropy is not violated in the collision. A rapidly convergent Newton-Raphson procedure is used to determine γ at each grid point and time iteration. The relaxation distribution functions f_α^{eq} extremize the H function, Eq. (44), subject to the local conservation of mass and momentum. Most of the simulations reported here use the polynomial form of the relaxation distribution functions, Eq. (6), including the cubic terms. We shall consider the dependence of the ELB simulations on the choice of the different bit models D3Q15, D3Q19, and D3Q27, as well as the difference between using the polynomial form for the relaxation distributions, Eq. (6), over what we shall call the "entropic" form, Eq. (13). It should be noted that recently Chikatamarla *et al.* have also developed an ELB equation for the D3Q15 bit model [8].

The bare (or "molecular") viscosity in the Navier-Stokes equation is, from the one-parameter standard LB representation, Eq. (4),

$$\nu=\frac{1}{6}(2\tau-1),$$

while the effective viscosity for the two-parameter ELB representation is

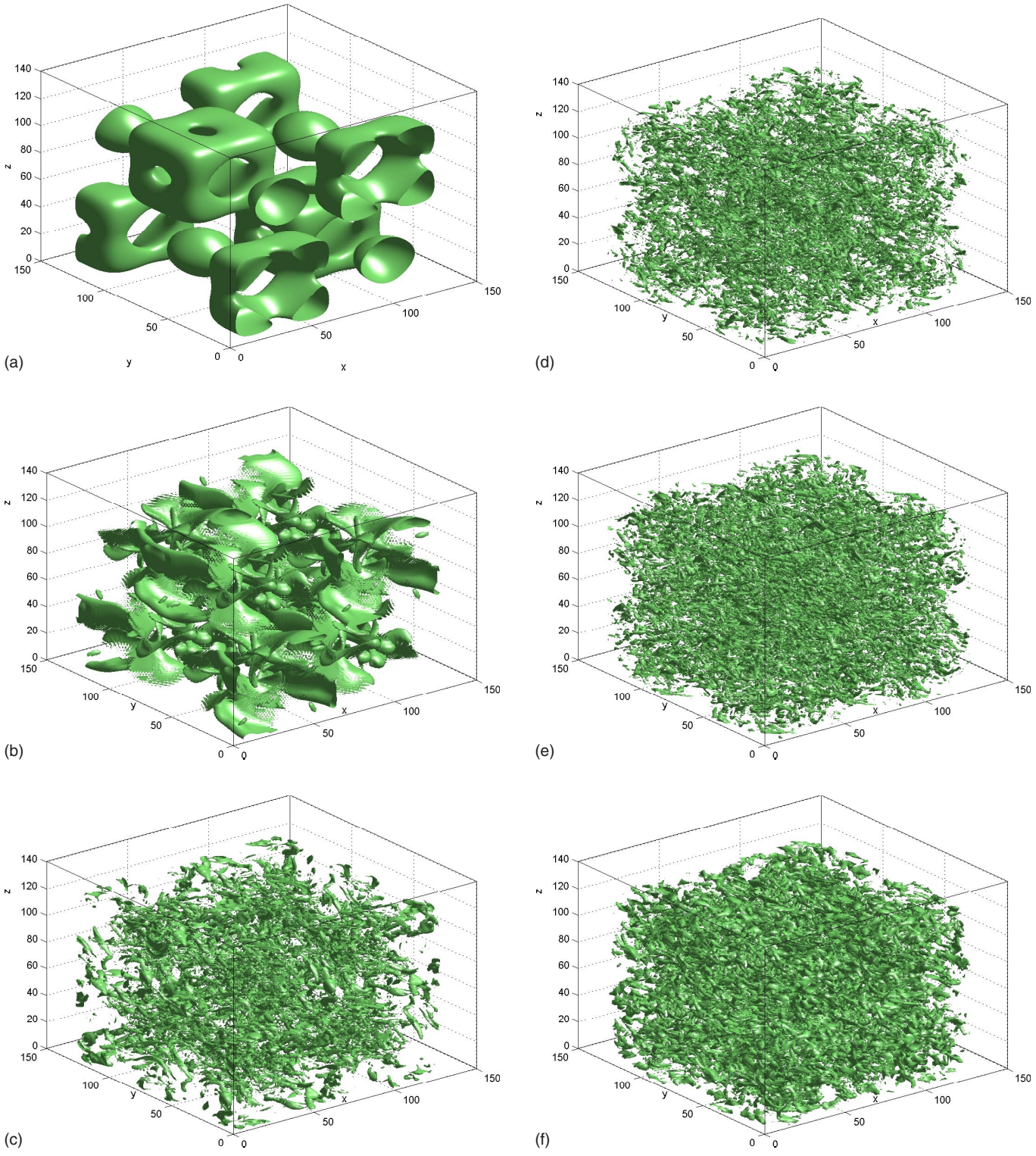

FIG. 4. (Color online) The evolution of the isosurface of $\tilde{\omega}_x(\mathbf{x},t)=0.15\omega_x(\mathbf{x},t)$ at (a) $t=0$, (b) $t=2.5$ K, (c) $t=5$ K, (d) $t=7.5$ K, (e) $t=10$ K, and (f) $t=15$ K, for the ELB D3Q27 model at viscosity $\nu=2\times10^{-3}$. Some of the symmetries of the initial Kida velocity profile are evident in the 15% isosurfaces at $t=0$ (a). The vortex stretching is seen in (b), followed by the breakup of these vortex structures in (c)–(e).

$$\nu_{eff}(\mathbf{x},t)=\frac{1}{6}\left(\frac{4\tau}{\gamma(\mathbf{x},t)}-1\right). \tag{49}$$

As $\tau\to0.5_+$, $\nu\to0$, the Reynolds number $\mathrm{Re}=U_0L_0/\nu\to\infty$, and the standard LB equation becomes violently unstable numerically. In the limit $\gamma(\mathbf{x},t)\equiv2$, the ELB equation reduces to the standard LB equation, but the ELB equation remains unconditionally stable as $\mathrm{Re}\to\infty$.

We consider free-decaying 3D Navier-Stokes turbulence, showing the evolution of the energy and entrophy as well as

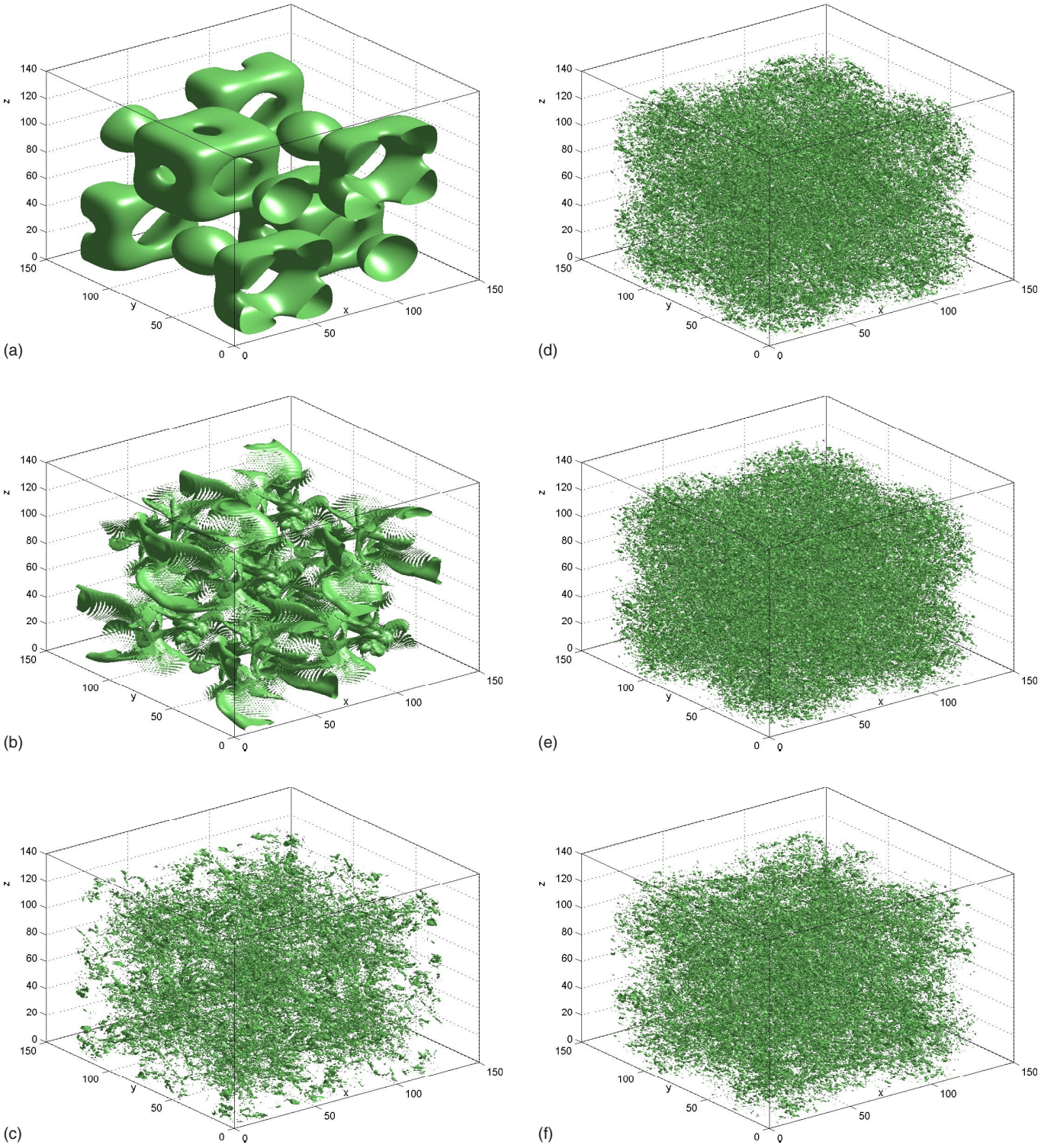

FIG. 5. (Color online) The evolution of the isosurface of $\tilde{\omega}_x(\mathbf{x},t)=0.15\omega_x(\mathbf{x},t)$ at (a) $t=0$, (b) $t=2.5$ K, (c) $t=5$ K, (d) $t=7.5$ K, (e) $t=10$ K, and (f) $t=15$ K, for the ELB D3Q27 model at viscosity $\nu=2\times10^{-4}$. Following the vortex stretching there is a more rapid breakup into smaller vortex clusters due to the higher Reynolds number than in Fig. 4.

isosurfaces of ω_x (the x component of vorticity) for the LB and ELB models: D3Q15, D3Q19, and D3Q27. The initial incompressible velocity profile is chosen to be the Kida profile [18]. On a $(2\pi)^3$ grid,

$$u_1(x_1,x_2\,.\,x_3) = U_0 \sin x_1(\cos 3x_2\cos x_3 - \cos x_2\cos 3x_3)$$
$$= u_2(x_3,x_1,x_2) = u_3(x_2,x_3,x_1), \tag{50}$$

where the subscripts $(1,2,3)\leftrightarrow(x,y,z)$. This initial profile

has periodicity 2π in all three directions, antisymmetric with respect to planes $x_i=\pi$ $(i=1,2,3)$ and invariant under rotation of $\pi/2$ around the lines $x_i=x_{i+1}=\pi/2$. The simulations presented here are on a 512^3 grid with $U_0=0.05$ and with two choices of bare viscosities: $\nu=2\times10^{-3}$ and $\nu=2\times10^{-4}$. At viscosity $\nu=2\times10^{-3}$, the Reynolds number Re=2037, giving a resolution scaling $L_0/\ell_D\approx \mathrm{Re}^{3/4}\approx 300$, where ℓ_D is the Kolmogorov dissipation length scale. Thus the simulations at this viscosity are fully resolved on the 512^3 grid. At the lower viscosity $\nu=2\times10^{-4}$, Re=20 370 so that the simulations are somewhat under-resolved on a 512^3 grid since $L_0/\ell_D\approx \mathrm{Re}^{3/4}\approx 1700$. The relaxation distribution functions used in these simulations is the polynomial form, Eq. (6).

In Figs. 1 and 2, we plot the kinetic energy E and enstrophy Ω,

$$E=\frac{1}{2}\int d^3x\mathbf{u}^2, \quad \Omega=\frac{1}{2}\int d^3x(\boldsymbol{\nabla}\times\mathbf{u})^2, \tag{51}$$

normalized to their initial value at $t=0$ for the two bare viscosities. For viscosity $\nu=2\times10^{-3}$, the normalized kinetic energy decay is very robust and almost independent of the chosen bit model (whether D3Q15, D3Q19, or D3Q27) and whether one is using the standard LB or ELB models, Fig. 1(a). However, the normalized enstrophy is much, more sensitive, Fig. 1(b). At early times ($t<3000$) there is an exponential growth in the enstrophy due to vortex stretching and growth of vortex filament strengths. As this is independent of viscosity, both LB and ELB simulations give the same enstrophy evolution for $t<3000$. This agreement is also independent of the bit model used. As the influence of the viscosity makes its mark on the turbulent flow, there are significant deviations between the models. Since the ELB approach introduces an effective viscosity, ν_{eff}, which is typically greater than the bare viscosity, the peak in the enstrophy (which is controlled by the viscosity) is greater for LB than for ELB simulations, as is seen in Fig. 1(b). For later times, there is polynomial decay of the enstrophy. On decreasing the viscosity to $\nu=2\times10^{-4}$; however, the LB algorithm rapidly becomes numerically unstable and so only the ELB results are shown in Fig. 2. Because of the lower viscosity (see Fig. 2), one finds an extended plateau of almost constant kinetic energy for $t<3000$ during the vortex stretching phase. There is also a stronger peaking in the enstrophy. The dependence on the number of streaming velocities (whether 15, 29, or 27 bits) is relatively mild.

The time evolution of $\max_{\mathbf{x}}\omega_x(\mathbf{x},t)$, the spatial maxima for the x component of the vorticity, is shown in Fig. 3 for viscosity $\nu=2\times10^{-3}$ [both LB, Fig. 3(a), and ELB, Fig. 3(b) flow] and for the lower viscosity $\nu=2\times10^{-4}$ [only ELB flow, Fig. 3(c), since the LB flow is now numerically unstable] for the various bit models. The early very rapid rise in ω_x is due to the nearly inviscid vortex stretching, and this rise is independent of the bit model chosen in the simulation. It is evident that the peak in these maxima is controlled by the viscosity. For lower viscosity, Fig. 3(c), the subsequent decay is essentially independent of the bit model while the higher-viscosity runs, Figs. 3(a) and 3(b), show more dependence on the bit model.

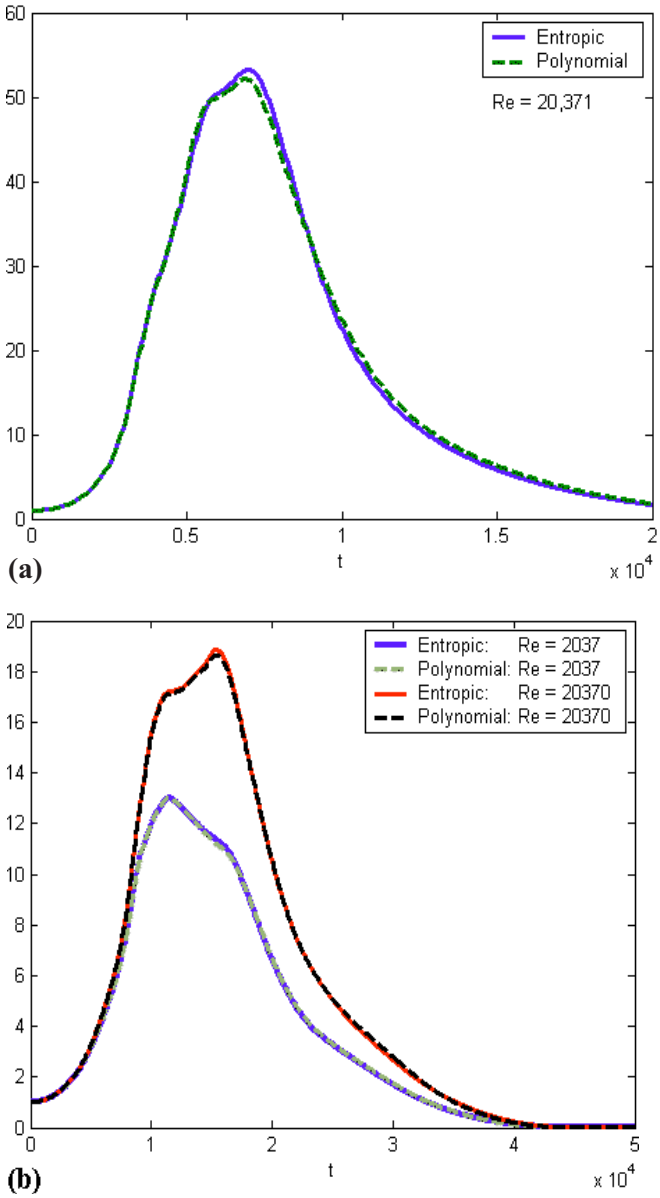

FIG. 6. (Color online) The effect of the choice of the relaxation distribution function on the normalized enstrophy for different Reynolds and Mach numbers for the D3Q27 model. There is little difference between the use of the standard polynomial relaxation distribution function [including $O(u^3)$ terms], Eq. (6), to the entropic form, Eq. (13), even at high Reynolds. This difference is nearly totally reduced when the Mach number is decreased from (a) Ma =0.086 to (b) Ma=0.035. The number of time iterations scales as U_0^{-1} so that lower-Mach-number simulations required longer-time runs.

In Figs. 4 and 5 we present the isosurfaces of ω_x at 15% of the $\max_{\mathbf{x}}\omega_x(\mathbf{x},t)$ at time snapshots $t=0$, 2.5, 5, 7.5, 10, and 15 K for the D3Q27 model. Vortex stretching is very evident at $t=2.5$ K [Figs. 4(b) and 5(b)] and at the lower viscosity these vortex structures break apart quicker (Fig. 5) than at the higher viscosity (Fig. 4).

Finally, in Fig. 6, we consider the effect of the form of the relaxation distribution, whether polynomial, Eq. (6), or "entropic," Eq. (13), on the normalized enstrophy for the D3Q27

model. For $U_0=0.05$ (i.e., Mach number Ma=0.086) and Re=20 370, the entropic form of the relaxation distribution function leads to a slightly higher enstrophy maximum than from the polynomial form. However, even this somewhat minor difference disappears at lower Mach number (Ma =0.035) with $U_0=0.02$, with the enstrophy being plotted at both Re=20 370 and Re=2037. Of course, the number of time iterations scales inversely with the Mach number, so that low-Mach-number simulations are somewhat more expensive computationally.

VI. CONCLUSION

In this paper we have examined the two seemingly different approaches to entropic lattice Boltzmann algorithms: one from the Zurich school [3–8] and the other from the Boston school [9–12]. Moreover, we have extended and completed the unification attempt started by Boghosian [14]. To recover the Navier-Stokes equation, one must include the constraint that the pressure tensor be independent of the fluid flow [18]. With this extra constraint, we have shown from first principles that the only appropriate entropy function is the (discrete) Boltzmann H function. Thus for Burgers turbulence, in which there is no pressure term, the entropy function is non-Boltzmann-like, as shown recently by Boghosian *et al.* [19].

We have also shown that though the entropic relaxation function determined by the Zurich school [3–8] is strictly valid for Navier-Stokes flow for the D3Q27 bit model, its moments [up to terms of $O(u^4)$] are the same as for the standard polynomial LB equilibria that have been in use for many years for both the D3Q19 and D3Q15 models [1]. In the 3D 512^3 grid simulations presented here the polynomial form of f_α^{eq} is used, but tests on the D3Q27 model have indicated only a very slight dependence on the form chosen f_α^{eq}—and this dependence disappears for lower Mach number. We have also compared the ELB and standard LB models. At viscosities where LB simulations are numerically stable, one finds somewhat higher peaks in the enstrophy in the standard LB models since ELB model introduces a renormalized and locally somewhat higher viscosity ν_{eff}, Eq. (49), than the bare molecular viscosity, Eq. (4), in the LB model. However, ELB simulations are unconditionally stable at any bare viscosity so that the only impediment is now grid resolution. Finally, we have started to consider the effect of the number of bits in the model, whether D3Q15, D3Q19, or D3Q27. The reduction in the number of bits leads to lower memory and run time requirements but at the expense of a lower level of discrete lattice symmetry. Our first simulation results seem to indicate relatively minor distortions due to lowering the lattice symmetry, particularly at higher Reynolds numbers, and this is presently under investigation.

ACKNOWLEDGMENTS

This work was supported by the AFOSR, AFRL, and DOE, using computer facilities at NERSC (DOE), NAVO (DOD), and ERDC (DOD).

[1] S. Succi, *The Lattice Boltzmann Equation for Fluid Dynamics and Beyond* (Clarendon Press, Oxford, 2001), and references therein.
[2] J. Carter, M. Soe, L. Oliker, Y. Tsuda, G. Vahala, L. Vahala, and A. Macnab (unpublished); G. Vahala, J. Carter, M. Soe, J. Yepez, L. Vahala, and A. Macnab, in *Parallel CFD 2005*, edited by A. Deane *et al.* (Elsevier, 2006).
[3] I. V. Karlin, A. Ferrante, and H. C. Ottinger, Europhys. Lett. **47**, 182 (1999).
[4] S. Ansumali and I. V. Karlin, Phys. Rev. E **62**, 7999 (2000).
[5] S. Ansumali and I. V. Karlin, Phys. Rev. E **65**, 056312 (2002).
[6] S. Ansumali, I. V. Karlin, and H. C. Ottinger, Europhys. Lett. **63**, 798 (2003).
[7] S. Ansumali and I. V. Karlin, Phys. Rev. Lett. **95**, 260605 (2005).
[8] S. S. Chikatamarla, S. Ansumali, and I. V. Karlin, Phys. Rev. Lett. **97**, 010201 (2006).
[9] B. M. Boghosian, J. Yepez, P. V. Coveney, and A. Wagner, Proc. R. Soc. London, Ser. A **457**, 717 (2001).
[10] B. M. Boghosian, P. J. Love, J. Yepez, and P. V. Coveney, Physica D **193**, 169 (2004).
[11] B. M. Boghosian, P. J. Love, P. V. Coveney, I. V. Karlin, S. Succi, and J. Yepez, Phys. Rev. E **68**, 025103(R) (2003).
[12] B. M. Boghosian, P. J. Love, and J. Yepez, Philos. Trans. R. Soc. London, Ser. A **362**, 1691 (2004).
[13] *Nonextensive Entropy*, edited by M. Gell-Mann and C. Tsallis (Oxford University Press, Oxford, 2004); C. Tsallis, J. Stat. Phys. **52**, 479 (1988).
[14] B. M. Boghosian, in *Complexity, Metastability and Nonextensivity*, edited by C. Beck, G. Benedek, A. Rapisarda, and C. Tsallis (World Scientific, Singapore, 2005), pp. 185–193.
[15] H. Chen, R. Zhang, I. Staroselsky, and M. Jhon, Physica A **362**, 125 (2006).
[16] M. Antoni and S. Ruffo, Phys. Rev. E **52**, 2361 (1995).
[17] Incidentally, the D3Q21 model, in which there are no speed-1 velocities so that $w_1 \equiv 0$, violates the requirement $w_\alpha \geqslant 0$, and so will not yield a valid ELB model.
[18] S. Kida and Y. Murakami, Phys. Fluids **30**, 2030 (1987).
[19] B. M. Boghosian, P. J. Love, and J. Yepez, Philos. Trans. R. Soc. London, Ser. A **362**, 1667 (2004).